TU Delft

Delft University of Technology

Quantifying the impacts of synoptic weather patterns on North Sea wind power production and ramp events under a changing climate

Cheneka, Bedassa R.; Watson, Simon J.; Basu, Sukanta

DOI
10.1016/j.egycc.2023.100113

Publication date
2023

Document Version
Final published version

Published in
Energy and Climate Change

Citation (APA)
Cheneka, B. R., Watson, S. J., & Basu, S. (2023). Quantifying the impacts of synoptic weather patterns on North Sea wind power production and ramp events under a changing climate. *Energy and Climate Change*, *4*, Article 100113. https://doi.org/10.1016/j.egycc.2023.100113

Important note
To cite this publication, please use the final published version (if applicable).
Please check the document version above.

Copyright
Other than for strictly personal use, it is not permitted to download, forward or distribute the text or part of it, without the consent of the author(s) and/or copyright holder(s), unless the work is under an open content license such as Creative Commons.

Takedown policy
Please contact us and provide details if you believe this document breaches copyrights.
We will remove access to the work immediately and investigate your claim.

This work is downloaded from Delft University of Technology.
For technical reasons the number of authors shown on this cover page is limited to a maximum of 10.

Energy and Climate Change 4 (2023) 100113

Contents lists available at ScienceDirect

Energy and Climate Change

journal homepage: www.sciencedirect.com/journal/energy-and-climate-change

Quantifying the impacts of synoptic weather patterns on North Sea wind power production and ramp events under a changing climate

Bedassa R. Cheneka [*,a], Simon J. Watson [a], Sukanta Basu [b]

[a] Wind Energy Section, Faculty of Aerospace Engineering, Delft University of Technology, 2629 HS Delft, the Netherlands
[b] Atmospheric Sciences Research Center, University at Albany, Albany, USA

ARTICLE INFO

Keywords:
Climate change
CORDEX
North Sea
Self-organizing maps
Wind ramps

ABSTRACT

Only a few studies on the overall impact of climate change on offshore wind power production and wind power ramps in the North Sea region have been published. This study focuses on the characteristics of expected wind power production and wind power ramps in the future climate aided by the classification of circulations patterns using a self-organizing map (SOM). A SOM is used to cluster high-resolution CMIP5-CORDEX sea level pressure data into 30 European area weather patterns. These patterns are used to better understand wind power production trends and any potential changes. An increased frequency of occurrence and extended persistence of high pressure systems lasting at least 24 h is projected in the future. Whereas a contrasting reducing tendency for low-pressure systems is estimated. No significant evidence is seen for a change in wind power capacity factor over the North Sea, though tentative evidence is seen for a reduction in wind power ramps. Annual energy production is seen to be dominated by a small number of weather patterns with westerly, south-westerly or north-westerly winds. Future wind power production is projected to become less from westerly winds and more from south-westerly and north-westerly flows. Ramp up events are primarily associated with strong south-westerly winds or weather patterns with a weak pressure gradient. Ramp down events have a stronger association with more north-westerly flow. In a future climate, a reduction in ramp up events associated with weak pressure gradients is projected.

1. Introduction

Renewable energy generation will play a significant role in the aspiration to limit global temperature change to 1.5°;C above pre-industrial levels [1]. The world needs a clear strategic plan to rapidly shift from fossil fuels to cleaner, renewable energy sources. As a result, European countries have been increasingly investing in developing renewable energy sources, primarily solar and wind energy. Offshore wind energy, in particular, has seen rapid growth in European waters. Cumulative offshore wind power capacity was 2.5 GW in 2009 but had reached 29.4 GW by August 2022 [2,3]. The North Sea, Irish Sea, Baltic, and Atlantic Ocean have the greatest potential for European offshore wind power production. Overall, a significant proportion of offshore wind power is obtained from the North Sea, accounting for 77% (16.9 GW) of the total European offshore wind power production [2]. As offshore wind will contribute an increasing fraction of future energy needs, there is now interest in how climate change may affect the level and characteristics of wind power production and wind power ramps, as this may have implications for future development and electricity grid balancing.

Studies have shown that projected changes in future wind speed patterns are highly uncertain, and there are significant disagreements between different climate models in [4–8]. For example, the change in the 50-year return period of near-surface wind speeds down-scaled from the Bergen Climate Model (BCM) by the Rossby Centre Regional Climate Model (RCA, ver.3 or RCA3) shows a significantly larger change than when down-scaled using the High-Resolution Limited Area Model (HIRHAM5) over the eastern and central Mediterranean [4]. This disagreement appears to be due to the poor choice of roughness length in the planetary boundary layer scheme in RCA3 [9]. Moreover, in [4], it is also shown that climate model uncertainty propagates from general circulation models (GCMs) to regional climate models (RCMs), which leads to spatial variation in the down-scaled projected wind speed change. Significant spatial differences are observed in the projected changes to the 50-year return period of wind speed values when using the ECHAM5 GCM compared with the Bergen Climate Model (BCM)

* Corresponding author.
E-mail address: b.r.cheneka@tudelft.nl (B.R. Cheneka).

https://doi.org/10.1016/j.egycc.2023.100113
Received 31 January 2023; Received in revised form 12 June 2023; Accepted 17 July 2023
Available online 20 July 2023
2666-2787/© 2023 The Authors. Published by Elsevier Ltd. This is an open access article under the CC BY license (http://creativecommons.org/licenses/by/4.0/).

when downscaled by the same RCM (HIRHAM5). The downscaled ECHAM5 predicts larger changes over the North Atlantic Ocean than the downscaled BCM. In contrast, the down-scaled BCM predicts greater changes over the Black Sea.

As well as future climate-driven changes to wind speed, a number of studies (e.g. in [10–15]) have considered how this might translate to changes in wind power in Europe. One such study has suggested that wind power production will increase over much of northern-eastern Europe, with the largest increases seen in the Baltic Sea. However, a decrease is seen for Atlantic areas, and much of western and southern Europe [11] and over the central Mediterranean Sea [12]. Here too, there is significant disagreement between different models regarding the sign of wind power changes. The work by [11] has shown that European wind power production is expected to show a change of about ± 15% and ± 20% by the mid and late 21st century, respectively [11]. A further study found that the production of wind power derived from the down-scaling of several GCMs using RCA (ver.4) for the Representative Concentration Pathway (RCP 4.5) and RCP 8.5 scenarios [16] shows a generally decreasing trend over the continent of Europe, with the exception of a slight increase over the Baltic Sea region [15].

Aside from spatial variation, projected changes in wind speed also show seasonal dependence. Some studies have indicated an increasing trend in wind power production during Winter, particularly over central and north-western Europe, while wind power production during the summer may decrease [6,14,17]. A model ensemble of down-scaled ECHAM5 output also shows similar seasonal behavior at the end of the 21st century over northern Europe [13,18]. In the European winter, wind power production is at full capacity for a significant amount of the time. By contrast, during the summer, the output is more often at partial load or around cut-in. Higher winds in Winter may have little impact on output or indeed require more curtailment in times of high production and low demand. In contrast, during the summer, lower winds may require more backup capacity from other sources or increased energy storage [14].

Changes in the future temporal variation in wind power, such as wind power ramps, associated with rapid changes in wind speed, could impact supply and integration into the grid. Few studies have been carried out to quantify potential changes in future wind power ramps. A study conducted in Japan projected a significant reduction in ramp down events under a high warming scenario, with the largest reduction in all ramp events during the autumn [19]. However, to date, there has been no similar study for Europe or the projected European offshore wind power fleet. This is the motivation for this present study which looks at the change in the projected future frequency of wind power ramps over the North Sea region.

The characteristics of wind speed and wind speed ramps (along with the associated changes in wind farm output, including wind power ramps) can be associated with particular weather patterns. Therefore, future changes in large-scale synoptic circulation systems are of concern when wishing to understand potential changes in the characteristics of wind farm production. Such changes can manifest as a change in the frequency of particular weather patterns, a change in the mean spatial value of certain variables, or a shift in the position of a particular feature associated with a weather pattern, such as a high or low-pressure center.

Studies have indicated potential changes in the seasonal mean of mean sea level pressure (MSLP) under a future climate [5,20,21]. For instance, in winter (DJF), the projected MSLP over the Mediterranean region shows an increasing trend, while any change is expected to be small in summer (JJA) [5]. It was shown that the seasonal change in MSLP could contribute to a decrease in wind speed during winter over this region but that the signal was unclear in summer. Therefore, exploring the projected changes in weather patterns could help to understand the factors contributing to wind speed, wind power, and power ramps under the influence of future climate change.

A self-organizing map (SOM) has been used widely for identifying weather patterns in the field of meteorology [22] showing itself to be a powerful tool for reducing data dimensions. SOMs have the advantage that similar patterns remain close to each other in the output map. Previously, SOMs have been used to identify prevailing weather patterns over Europe [23,24], and it was shown that SOM-based weather patterns captured the dominant circulation systems which could then be used to study spatial and temporal wind speed trends. Based on these findings, the approach taken in this work is to use a SOM to identify 30 distinct weather patterns using historical and projected sea level pressure data. The map is then used to study changes in the prevalence of each pattern and the impact this may have on future projected mean wind speed, wind power and ramp event frequency.

Specifically, the objectives of this study are: (i) to identify European weather patterns using three-hourly MSLP data from multiple climate model for 1970–2077, (ii) to quantify changes in the prevalence of these patterns in the 2006–2041 and 2042–2077 periods compared with the base period, 1970–2005 and (iii) to quantify the impact any changes may have on mean wind speed, wind power and wind power ramps events under future projected climate change.

2. Data

This study uses near-surface wind speed and MSLP data from downscaled GCMs, Coordinated Regional Downscaling Experiment (CORDEX). CORDEX was a globally coordinated project that produced simulated future climate data using several GCMs which were then downscaled using different RCMs. Different initialization states and physical parameterizations were used to generate ensemble predictions of the future climate. The aim of the CORDEX project was to generate regional-scale climate projections for impact assessment and adaptation studies worldwide, and the data are available from the Earth System Grid Federation (ESGF) LIU portal [25]. The European CORDEX (EU-CORDEX) model outputs which are available at a spatial resolution of 0.11 degrees (EUR-11, 12.5 km) and three-hourly temporal resolution are used in this study [26]. In total, output data from six RCA (ver 4.1) downscaled GCMs for the historical period 1970–2005 and the future period from the Coupled Model Intercomparison Project Phase 5 (CMIP5), 2006 – 2077 are used (Table 1). CMIP5 projections are made using different Representative Concentration Pathway (RCP) scenarios, and in this study, the medium RCP scenario, RCP4.5, is used. The RCP4.5 scenario results in an increase of global temperature of about 2°C at the end of 21^{st} century [27]. The dataset is split into three periods, 1970 – 2005 (referred to henceforth as P-0), 2006 – 2041 (P-I), and 2042 - 2077 (P-II).

For this study, wind speed and wind power values were calculated based on the three-hourly data for each of the six models in Table 1. These values were also averaged over the six models and are henceforth referred to as ensemble averages.

3. Methods

3.1. Wind power estimation

The CORDEX wind speed speed data are provided at 10 m above the surface. The wind speed is extrapolated to a hypothetical turbine hub height of 100 m using the log law following the example of other researchers e.g. [35]. The surface roughness length is chosen as 0.0002 m to be representative of open sea as this work is primarily focused on offshore wind power.

The extrapolated wind speed value is used to estimate wind power production by using a hypothetical 8 MW power curve [36]. The power curve has a cut-in wind speed of 4 m/s, a rated wind speed of 12.5 m/s, and a cut-out wind speed of 25 m/s. To simplify the analysis of wind power production and wind power ramps characters, the wind power is normalised to the rated power to generate a capacity factor.

3.2. Detection of wind power ramps

The detection of wind speed ramps and wind power ramps is challenging given that there is no agreed definition of what actually is a ramp or how to distinguish a ramp from uncorrelated random fluctuations. In the literature, several ramp detection algorithms have been proposed in recent years [37–41]. In [37], a novel approach was proposed employing wavelets in conjunction with randomly shuffled surrogates. The approach was illustrated using observational data from the Belgian aggregated offshore wind farms. We have adopted this approach for the present study which involves using a wavelet transformation of a time series of wind power capacity factor values and a large number of randomly shuffled data realisations. The wavelet coefficients from the random realisations are used to discriminate the wavelet coefficients of the original time series based on a maximum wavelet scale ($a_{\max}$) and a discrimination level (W_T^*). In Fig. 1, four examples are shown for the detection of ramp events based on a maximum wavelet scale $a_{\max} = 20$ and four discrimination levels of W_T^*. It can be seen that by reducing the value of W_T^* from 10% to 1%, fewer ramps are detected. In this study, we use a discrimination level of $W_T^* = 5\%$ to provide a good balance between detecting a power ramp event whilst excluding uncorrelated random fluctuations.

3.3. Clustering of weather patterns

Based on the results of a previous study [24], we used a SOM to cluster three-hourly CORDEX MSLP data into 30 distinct weather patterns using the SOM_PAK software package [42]. The MSLP output data from each of the six downscaled GCMs for the full period, 1970 – 2077 (comprising P-0, P-I, and P-II datasets), were first concatenated. They were then fed into the software sequentially, and the SOM neuron weights initialized randomly from the spatial MSLP data. Sequential training was carried out in two phases. The first phase, known as rough training, was used to arrange the weight vectors of the SOM neurons topologically. This training phase used a large initial learning rate (α_0=0.05) and neighborhood radius size (σ_0=6). With training time, both values were decreased linearly as a function of iteration time which was set to about 400,000 time steps. In the fine-tuning phase, training was initialised using the output from the rough training phase. In this phase, a smaller initial learning rate (α_0=0.02) and neighborhood radius size (σ_0=3) were used which were also decreased linearly. Finally, a Sammon mapping projection [43] was used at different iteration steps until the neurons were not twisted, which indicated that the SOM was trained sufficiently. Once the topological order of the weight vectors was determined, the best matching unit corresponding to the input data was determined based on the minimum Euclidean distance between the weight of the neurons and the input data vectors.

4. SOM-based weather patterns

Fig. 2(a) shows the 30 generated weather patterns. Due to the nature of a SOM, similar circulation systems cluster close together on a map. Many weather patterns show distinct circulation types, *e.g.*, cyclonic, anti-cyclonic, zonal, and meridional flow. At the top of the map, the weather patterns are dominated by meridional flow (b1) and high-pressure systems (c1, d1, e1, and f1). Weather patterns at the bottom of the map are mainly characterised by low-pressure systems (a5 – d5). Weather patterns to the left of the map are mainly characterised by northeasterly flow (a1 and a3) with low pressure over Scandinavia. Weather patterns on the right are characterised by southwesterly flow (f4 and f5) with high pressure over the European continent and Scandinavia. The most distinct weather pattern systems are located at the edges of the map.

Fig. 2(b) shows the percentage frequency of occurrence of each weather pattern. Fig. 2(c) shows the distribution of the duration of weather pattern events based on consecutive three-hourly values for weather patterns d1, c2, b5, and f5. The longest weather pattern events persist for 14 days but those that persist more than six days are rare. Furthermore, Fig. 2(d) shows the percentage fraction (Frac) of events by weather pattern that persist for at least 24 h, *i.e.* nine or more consecutive three-hourly values. This is given by the fraction of weather pattern events to the right of vertical dashed blue line in Fig. 2(c). Weather patterns located at the edges of the map such as weather patterns b5, f5, a3, d1, and a2 tend to occur more frequently and with greater persistence than the weather patterns at the center. These outer weather patterns tend to be associated with quite distinct circulation features with relatively strong pressure gradients. The central weather patterns display weaker pressure gradients, and their lower persistence suggests that they are more likely to be transition states between the outer weather patterns in the map.

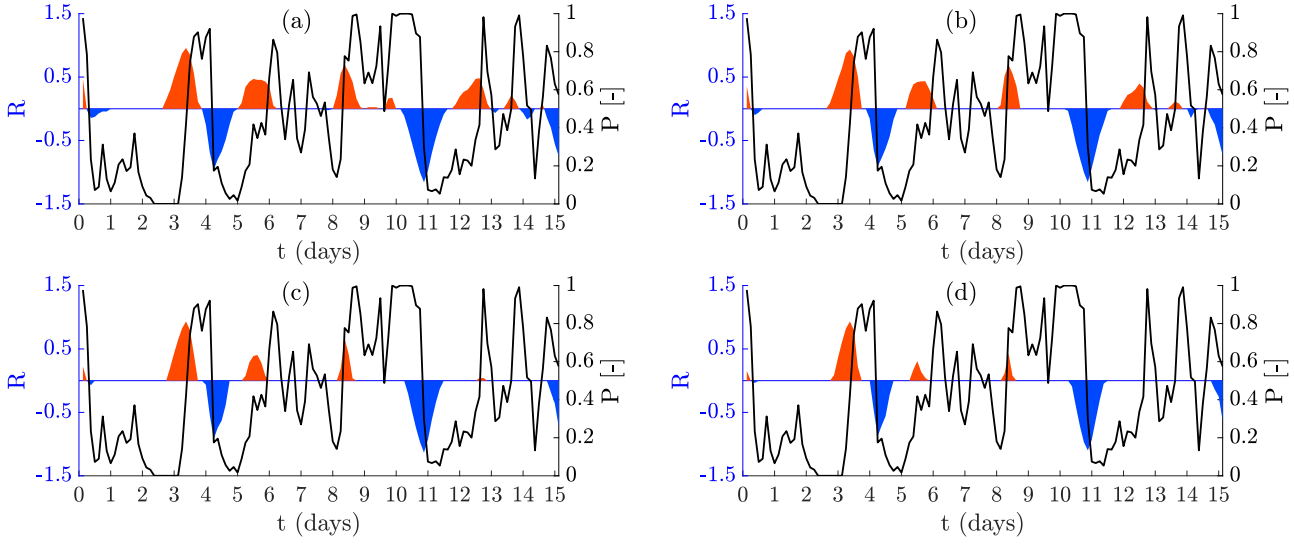

Fig. 1. Normalised wind power ramps (R) from 15 to 31 December 2005 based on a sample of three-hourly CORDEX downscaled CNRM data. Ramps are detected using a wavelet-surrogate method with a maximum wavelet scale value of $a_{\max}$=20 and discrimination levels, W_T^* of: (a) 10% (b) 5% (c) 2% and (d) 1%. Ramp up events are shown in red and ramp down events in blue.

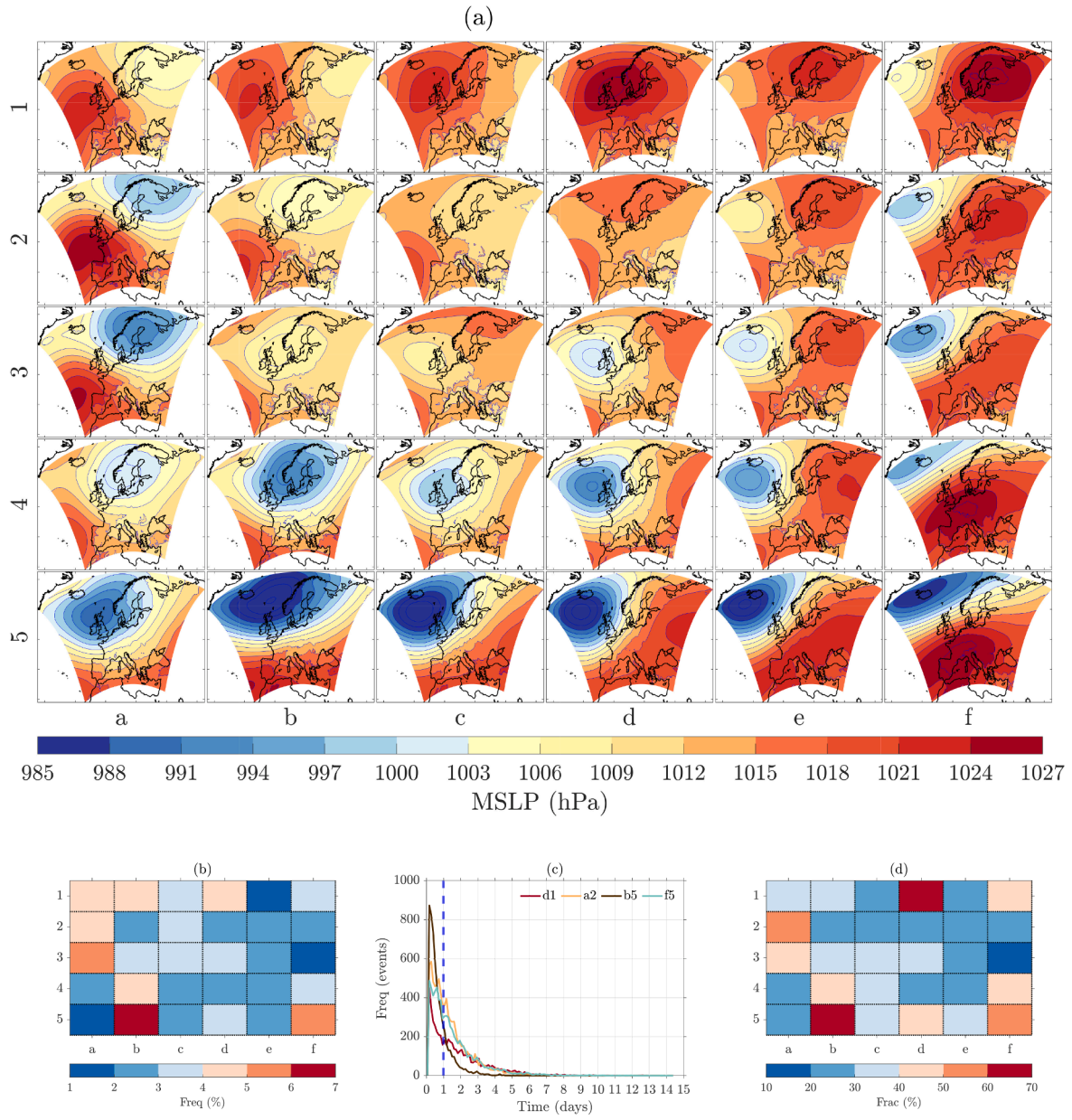

Fig. 2. SOM-based weather patterns: (a) clusters based on three-hourly MSLP, 1970 – 2077. The shaded color is the MSLP in hPa and the contour line is MSLP in 3hPa intervals, (b) frequency of occurrence in (%), (c) distribution of the duration of events corresponding to weather patterns d1, a2, b5, and f5, and (d) fraction (%) of events where a weather pattern persists at least 24 h. The vertical dashed blue line in (c) shows the threshold used to calculate the fraction of events in (d). N.B. The rows (1 – 5) and columns (a – f) are used to label weather patterns.

4.1. Projected future SOM-based weather patterns changes

Fig. 3(a) and (b) show the projected change of weather pattern frequency in P-I and P-II, respectively, relative to P-0. Overall, comparing the two future periods, the projected change of weather pattern frequency is greater in P-II compared to P-I. The weather patterns that are mainly located at the top and right are characterised by an increasing tendency, and the high-pressure and southwesterly flow characterises these weather patterns. On the other hand, most of the weather patterns that are located around the center and some of the weather patterns that are located at the bottom are characterised by a weak spatial pressure gradient and low-pressure systems. These weather patterns shows a decreasing tendency in the future climate.Fig. 3(c) and (d) show the change in the fraction of weather patterns which persist at least 24 h for the two periods, P-I and P-II, relative to P-0. Overall, a similar trend is seen, though some differences are seen near the top of the map. For example, weather patterns c1 and e1 show an increasing frequency based on all three-hourly values, whereas the corresponding weather patterns that persist at least 24 h show a decreasing trend for c1 and for e1 an increase in P-I and a decrease in P-II.

To further investigate the consistency of the temporal changes, trends are analysed on a yearly basis in Fig.4. Fig. 4(a) shows the change in weather pattern frequency per year over the entire study period based on all three-hourly values, and Fig. 4(b) shows the same information but for weather patterns persisting at least 24 h. Those patterns where the trend is significant at the 5% level are indicated. Weather patterns that are located at the left, top, and bottom right, with dominant high pressure systems centred to the west and south of Europe show a significant increasing trend, whereas those with a significant decreasing trend are located at the center and bottom of the map which tend to have a either weak pressure gradient or are dominated by low pressure systems centred to the west of Europe.

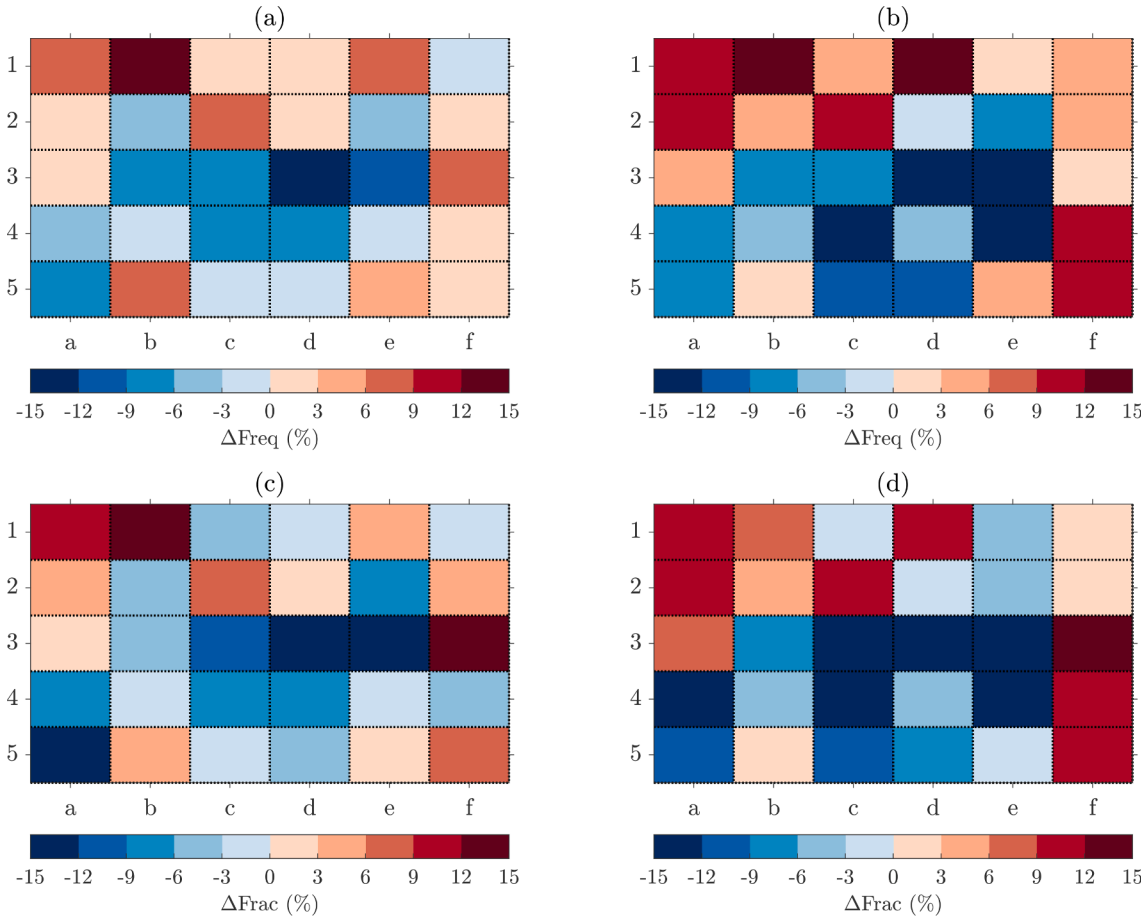

Fig. 3. Projected changes in SOM-based weather pattern occurrence relative to P-0: (a) change in weather pattern frequency in P-I, (b) same as (a) but in P-II; (c) change in the fraction of of events in P-I where a weather pattern persists at least 24 h; (d) same as (c) but in P-II.

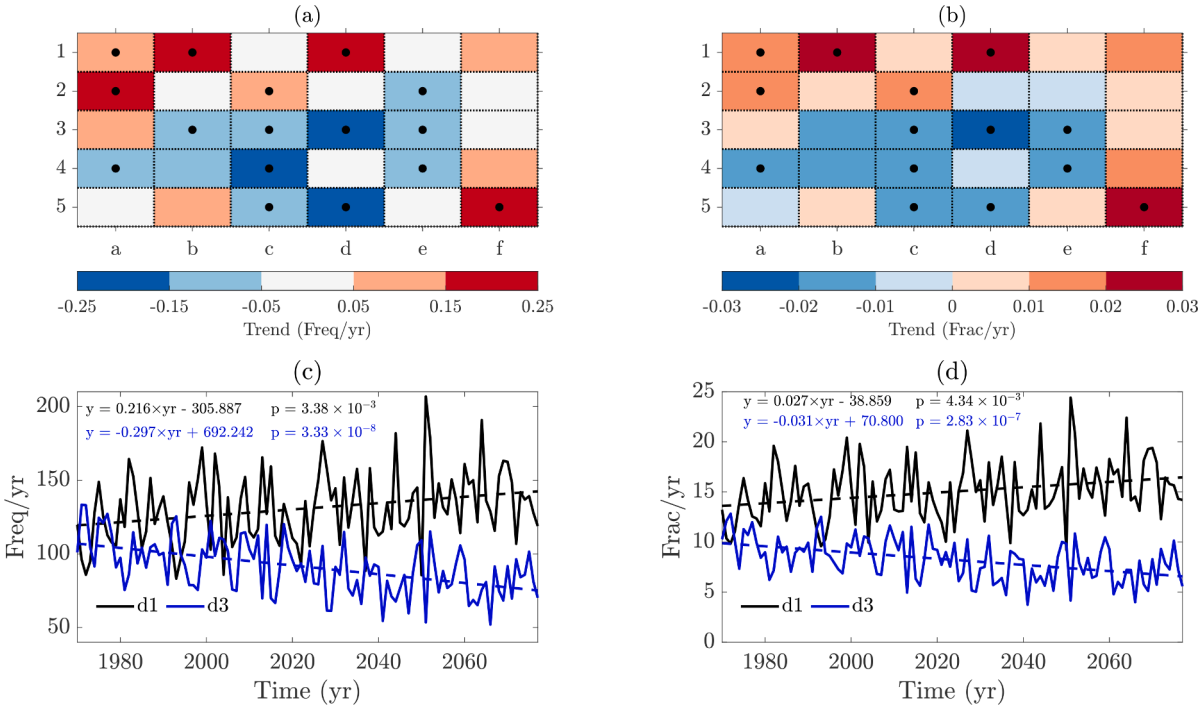

Fig. 4. Based on the entire study period: (a) change in weather pattern frequency per year based on all three-hourly data; (b) as (a) but for events of a particular weather pattern that persist for at least 24 h; (c) annual frequency/year for patterns d1 and d3 based on all three-hourly values; and (d) as (b) but for events of a particular weather pattern that persist for at least 24 h. The dots in (a) and (b) represent where the *p*-value of the trend <0.05.

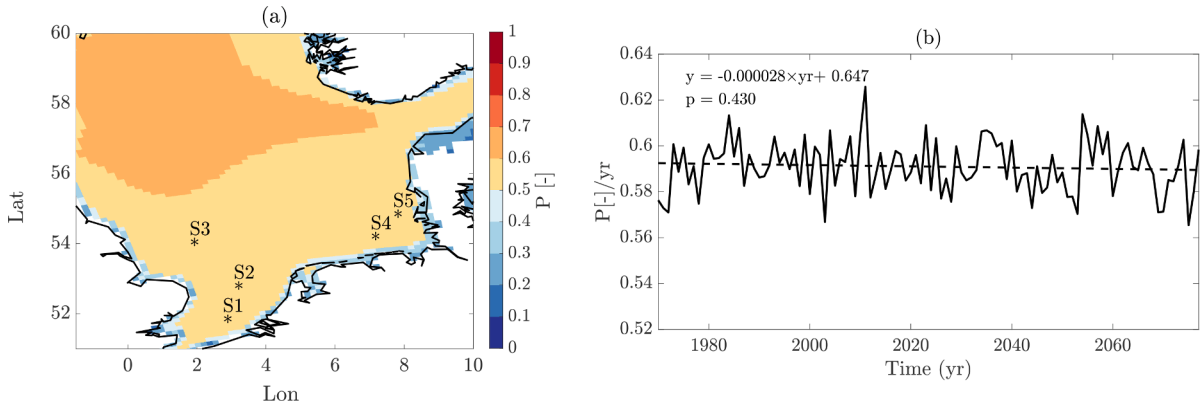

Fig. 5. (a) Spatial map of capacity factor based on mean wind speed values from the ensemble of the six downscaled models in Table 1 for P-0 showing grid points close to offshore wind farm locations S1–S5; and (b) yearly ensemble values of the capacity factor for S2 for the entire study period 1970–2077 showing the best fit linear trend and significance level.

Table 1
CORDEX downscaled GCMs by RCA (ver.4.1) and the downscaled ensemble members.

Driving Model	Calendar days	Ensemble[a]	References
CNRM-CERFACS-CNRM-CM5 (CNRM)	366	r1i1p1	[28]
ICHEC-EC-EARTH (ICHEC)	366	r12i1p1	[29]
IPSL-IPSL-CM5A-MR (IPSL)	365	r1i1p1	[30]
MOHC-HadGEM2-ES (MOHC)	360	r1i1p1	[31]
MPI-M-MPI-ESM-LR (MPI)	366	r1i1p1	[32]
NCC-NorESM1-M (NCC)	365	r1i1p1	[33,34]

[a] rN is the index of ensemble members, iN is the index of initialization states, and pN corresponds to the index of physical parameterizations used.

For two of the weather patterns that show a significant increasing and decreasing trends, a yearly plot is shown. Fig. 4(c) and (d) show the annual frequency per year of weather patterns d1 (a pattern dominated by high pressure) and d3 (a pattern with a relatively weak low pressure system) based on all values and where a pattern persists for at least 24 h, respectively. The trends are clear for both weather patterns though there is a large degree of inter-annual variation.

5. Future wind power production and wind power ramps

5.1. Projected changes in wind power production

Capacity factors were first calculated based on the wind speed values from each of the six downscaled models in Table 1 and then a mean of these values evaluated from the ensemble of the six. Fig. 5(a) shows the six-model ensemble capacity factor over the North Sea for P-0. Five grid points close to offshore wind farm locations are selected to analyze the temporal trend and variability of the wind power capacity factor over the North Sea area in more detail and these are marked on the map as: S1 (Belwind), S2 (Borssele), S3 (Hornsea 1), S4 (Gode Wind 1 and 2) and S5 (Horns Rev 3). In order to show the level of inter-annual variability, Fig. 5(b) shows the annual capacity factor and trend line over the period 1970 – 2077 for S2. For each of the sites S1 to S5, a trend line is fitted to the mean annual capacity factors and the slope along with the *p*-value of the fit (in brackets) is shown in Table 2. Where the *p* value of the slope is < 0.05, the values are highlighted in bold. For the capacity factors calculated based on the mean model ensemble wind speed values, there is no significant trend for any of the sites. For the downscaled ICHEC model, all sites show a significant decreasing trend and for the downscaled MPI model, two of the sites (S2 and S3) show a significant decreasing trend.

Fig. 6(a) and (b) show the change in MSLP over Europe for the P-I and P-II periods, respectively, compared with the base period. A progressive increase in pressure is seen over the Atlantic extending over the continent and the North Sea region with reducing pressure over north-eastern Europe.

Fig. 6(c–f) show the change in wind speed and capacity factor over the North Sea region for P-I and P-II relative to P-0 based on the mean six model ensemble wind speed values. For P-I, Fig. 6(c) shows an increasing trend in wind speed over the south, southeast, and east of the region and a decreasing trend over the north and northwest. By contrast, for P-II, Fig. 6(d) shows wind speed strongly decreasing over the north and northwest, and a weaker increase over the south, southeast and east of the region. This is consistent with the change in MSLP where during P-I, the increase in pressure in the Atlantic initially contributes to an increase in pressure gradient which then weakens over the western North Sea during P-II once the increase in pressure becomes more widespread over the continent. Fig. 6(e) and (f), show the corresponding projected

Table 2
The best-fit linear trend ($\times 10^{-5}$) and *p*-values based on the capacity factor over the entire study period for each model at sites S1 to S5. The text in bold indicates that the estimated slope is significant at $p < 0.05$ where the *p*-values are shown in parentheses.

Models	S1	S2	S3	S4	S5
Ensemble	− 1.8(0.656)	− 2.8(0.430)	− 8.0 (0.793)	− 2.1 (0.589)	− 5.0(0.890)
CNRM	16(0.116)	14.7(0.133)	11.9(0.185)	14.2(0.121)	10.6(0.230)
ICHEC	**− 22.4(0.013)**	**− 22.4(0.010)**	**− 22.2(0.009)**	**− 19.9(0.015)**	**− 24.2(0.03)**
IPSL	8.1(0.560)	4.9(0.654)	13.3(0.188)	19.0(0.102)	21.3(0.062)
MOHC	2.1(0.850)	3.4(0.750)	0.8(0.935)	5.0(0.635)	3.0(0.062)
MPI	− 17.0(0.053)	**− 24.0(0.004)**	**− 19.6(0.019)**	14.6(0.127)	16.4(0.091)
NCC	2.5(0.781)	6.7(0.425)	10.7(0.193)	8.7(0.373)	8.8(0.362)

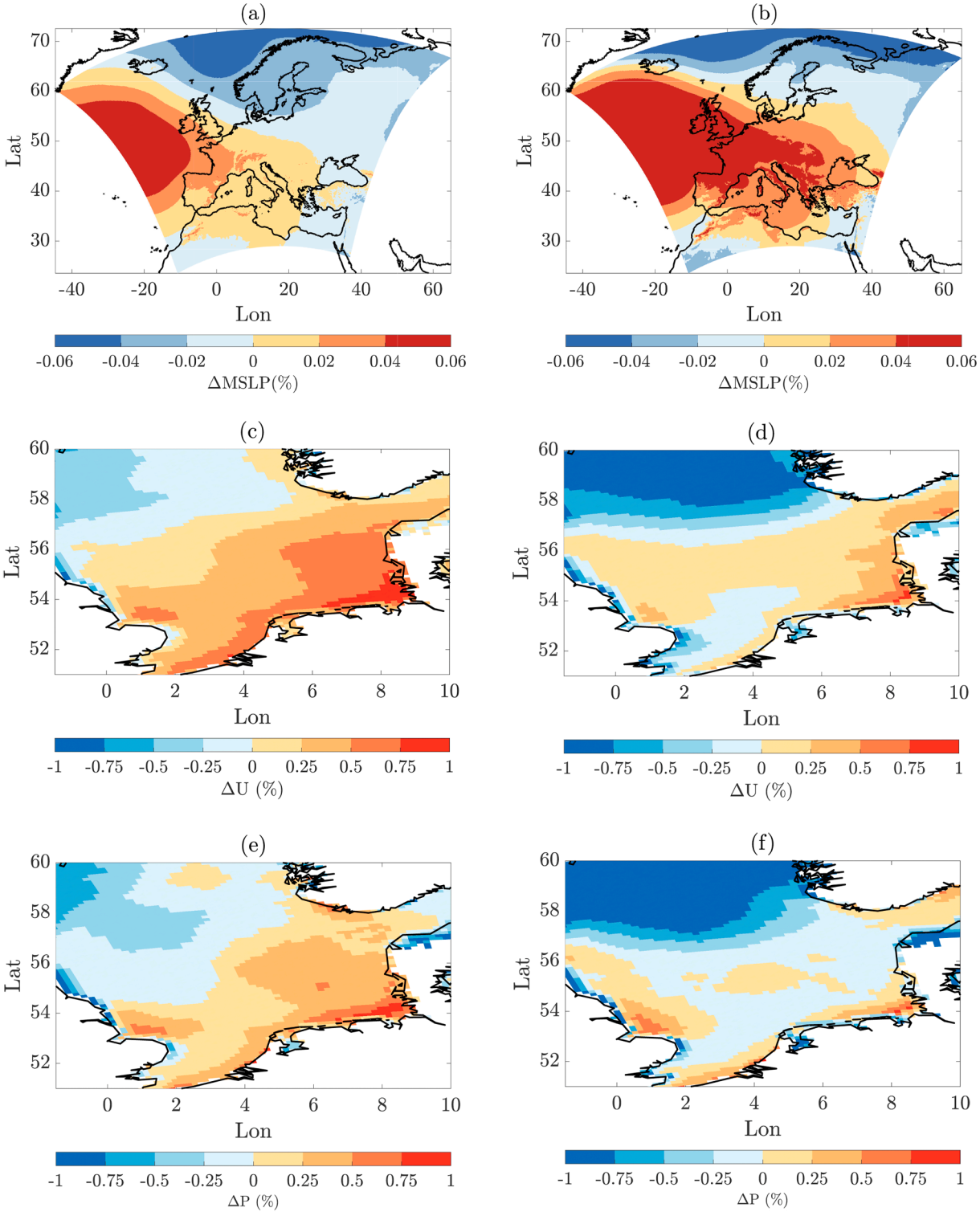

Fig. 6. Projected change relative to P-0 in: (a) average mean sea level pressure for P-I, (b) average mean sea level pressure for P-II, (c) average wind speed for P-I, (d) average wind speed for P-II, (e) average capacity factor for P-I, and (f) average capacity factor for P-II,. All values are based on mean values from an ensemble of the six models in Table 1.

changes in capacity factor for P-I and P-II, respectively. It can be seen that the trends are similar though slightly less pronounced than the spatial changes in wind speed due to the non-linear nature of the power curve where power output is constant over the range of wind speeds between rated and cut-out.

Fig. 7 compares the annual capacity factor for each model based on the grid point closest to S2. In each case, a best fit linear trend line is shown along with its p value. CNRM, IPSL, MOHC and NCC show no signicant trend, but ICHEC and MPI show declining values with p values < 0.05. It is also notable that IPSL gives annual capacity factor values which are significantly lower than the other models.

The best fit linear trend line and significant level (p) are calculated for all the sites S1 to S5 for the ensemble and individual models as shown in Table 2. The capacity factor based on the ensemble mean shows a

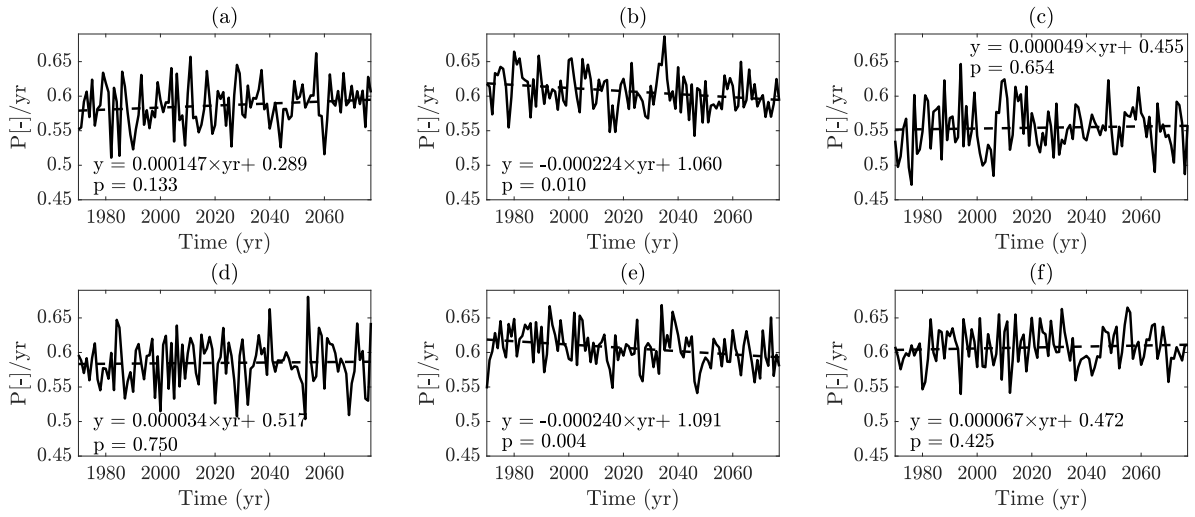

Fig. 7. For the grid point closest to site S2, the best fit trend-line, equations and *p*-value values of wind power capacity factor for models: (a) CNRM, (b) ICHEC, (c) IPSL, (d) MOHC, (e) MPI, and (f) NCC are shown.

declining trend for all sites though it is not significant. With the exception of ICHEC and MPI, all models show a slight increasing trend though this is not significant. ICHEC shows a significant declining trend ($p < 0.05$) for all sites and MPI shows a significant declining trend for S2 and S3. The disagreement between the models is likely associated with differences in GCM numerics and physical parameterizations which is outside the scope of this study.

5.2. Projected changes in wind power ramps

Wind power ramps were calculated following the procedure described in Section 3.2. First, the capacity factor was calculated for each model, then the total number of ramps per year was calculated for each model and from this an ensemble average was determined. Fig. 8(a-d) show spatial maps over the North Sea of the projected change in the ensemble averaged ramp up and ramp down frequency for P-I and P-II compared to P-0. The maps indicate a decreasing trend in wind power ramps over some of the North Sea region especially off the eastern coast of the UK and the Dutch coast. The trends for ramp up and ramp down events are similar. For site S2, the annual frequencies of ramp up and ramp down events are shown in Fig. 8(e) for the entire study period. The trend lines are clearly negative and significant at $p < 0.05$ despite some degree of interannual variability.

Fig. 9 shows the annual ramp frequency for each individual model

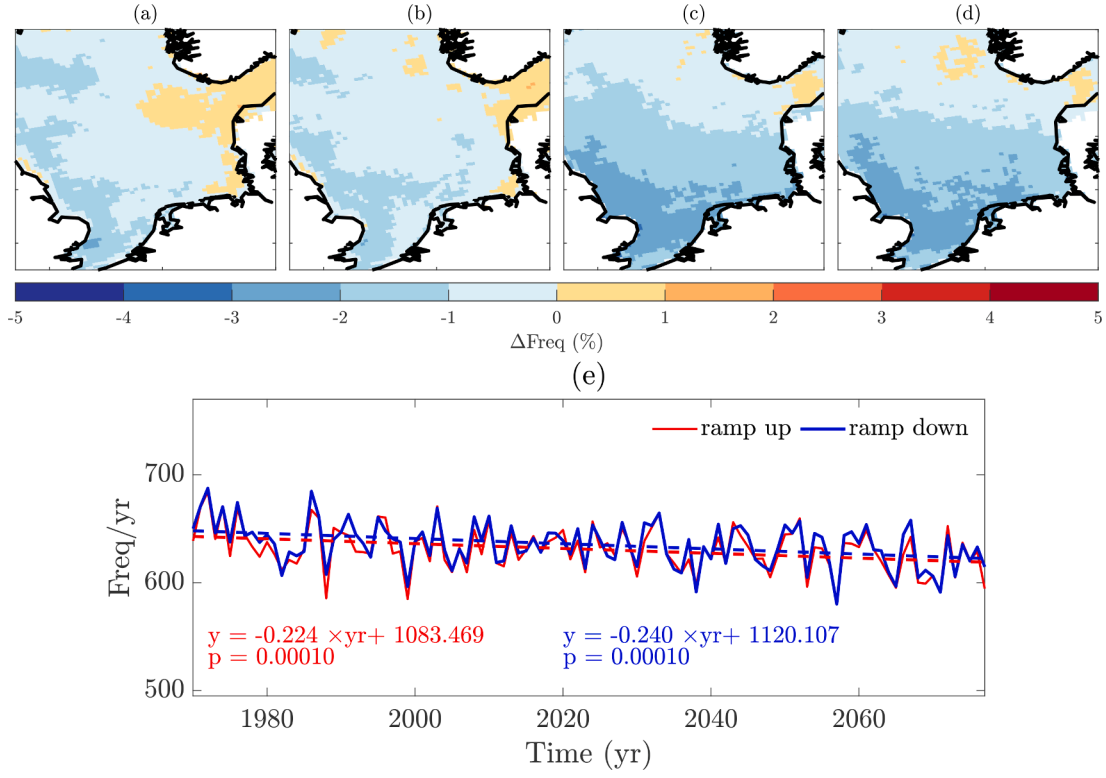

Fig. 8. Projected changes compared to P-0 in model ensemble wind power ramp frequency: (a) ramp up events for P-I, (b) as (a) but for ramp down events, (c) as (a) but for P-II, (d) as (c) but for ramp down events; and (e) annual ramp up and ramp down event frequencies at site S2 with best fit linear trend-line and *p*-value.

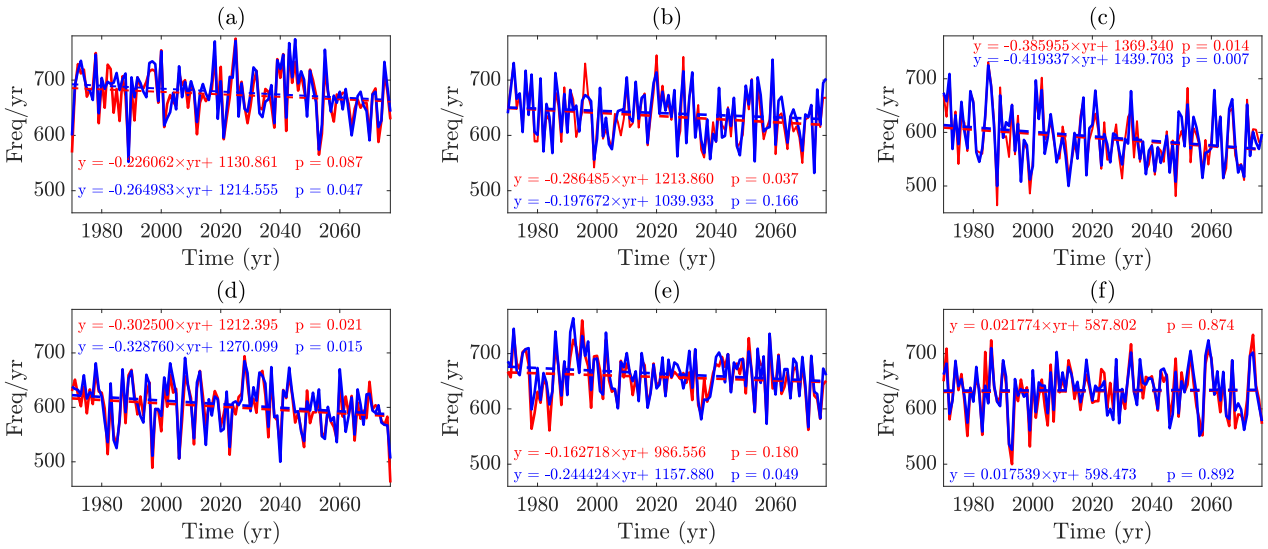

Fig. 9. Annual wind power ramp up (red) and ramp down (blue) event frequencies for site S2, with best fit linear trend line and *p*-value of estimated slope based on data from the models: (a) CNRM, (b) ICHEC, (c) IPSL, (d) MOHC, (e) MPI, and (f) NCC.

Table 3
Annual wind power ramp up frequency trend line slope and *p*-value (p) in parentheses by model for sites S1 to S5. The bold text indicates the estimated slope has a significant level $p < 0.05$.

	ramp up events				
Models	S1	S2	S3	S4	S5
Ensemble	**− 0.215(0.00004)**	**− 0.224(0.00010)**	**− 0.225(0.00047)**	**− 0.147(0.00175)**	**− 0.162(0.00984)**
CNRM	**− 0.327(0.016)**	− 0.226(0.087)	− 0.111(0.386)	− 0.035(0.796)	− 0.109(0.409)
ICHEC	− 0.161(0.223)	**− 0.286(0.037)**	**− 0.292(0.033)**	− 0.315(0.050)	**− 0.339(0.023)**
IPSL	**− 0.462(0.003)**	**− 0.386(0.014)**	**− 0.323(0.030)**	− 0.277(0.071)	− 0.209(0.187)
MOHC	**− 0.327(0.016)**	**− 0.303(0.021)**	− 0.222(0.110)	**− 0.375(0.010)**	**− 0.361(0.014)**
MPI	− 0.146(0.239)	− 0.163(0.180)	− 0.250(0.055)	− 0.052(0.652)	0.007(0.948)
NCC	0.133(0.313)	0.022(0.874)	− 0.154(0.256)	0.169(0.216)	0.042(0.747)

Table 4
Annual wind power ramp down frequency trend line slope and *p*-value (p) in parentheses by model for sites S1 to S5. The bold text indicates the estimated slope has a significant level $p < 0.05$.

	ramp down events				
Models	S1	S2	S3	S4	S5
Ensemble	**− 0.232(0.00004)**	**− 0.240(0.00010)**	**− 0.202(0.00047)**	**− 0.184(0.00984)**	**− 0.142(0.00984)**
CNRM	**− 0.352(0.013)**	**− 0.265(0.047)**	− 0.090(0.493)	− 0.044(0.739)	0.104(0.431)
ICHEC	− 0.133(0.344)	− 0.198(0.166)	− 0.244(0.077)	− 0.295(0.060)	**− 0.315(0.031)**
IPSL	**− 0.449(0.003)**	− 0.419(0.007)	**− 0.314(0.027)**	**− 0.368(0.020)**	− 0.127(0.411)
MOHC	**− 0.389(0.003)**	**− 0.329(0.015)**	− 0.187(0.187)	**− 0.373(0.008)**	**− 0.389(0.007)**
MPI	− 0.012(0.920)	**− 0.244(0.049)**	**− 0.312(0.017)**	− 0.172(0.149)	0.023(0.833)
NCC	− 0.058(0.651)	0.018(0.892)	− 0.062(0.641)	0.148(0.254)	0.062(0.620)

for site S2. All but one of the models (i.e., except NCC) show declining trends for ramp up and ramp down events over the study period. ICHEC, IPSL, and MOHC show significantly declining ramp up events with $p < 0.05$ and CNRM, IPSL, MOHC, and MPI show significantly declining ramp down events (there are some differences across the models in terms of the absolute number of ramp events with CNRM projecting the most and IPSL the least).

Tables 3 and 4 summarise the best fit trend line slopes to the annual ramp up and ramp down event frequencies, respectively, over the study period for each of the sites S1 – S5 by all the models and their ensemble. For all sites, the ensemble average trend shows a significant decline where the p value < 0.05. All of the sites show significant declining trends according to at least some of the models, though not the majority. The NCC model shows some evidence of increasing frequency at certain sites and site S5 (the most easterly site) also shows evidence of an increasing ramp up and ramp down frequency for some models, but neither of these trends is significant.

6. The impact of future weather pattern changes on wind power and wind power ramps

This section looks out how different weather patterns contribute to wind power production and wind power ramps and how this is projected to change in the future.

6.1. Impact on wind power

Fig. 10(a) shows how annual energy production (AEP) is distributed amongst the different weather patterns for S1 – S5. It is notable that a large fraction of the AEP (10%) is associated with pattern b5. This

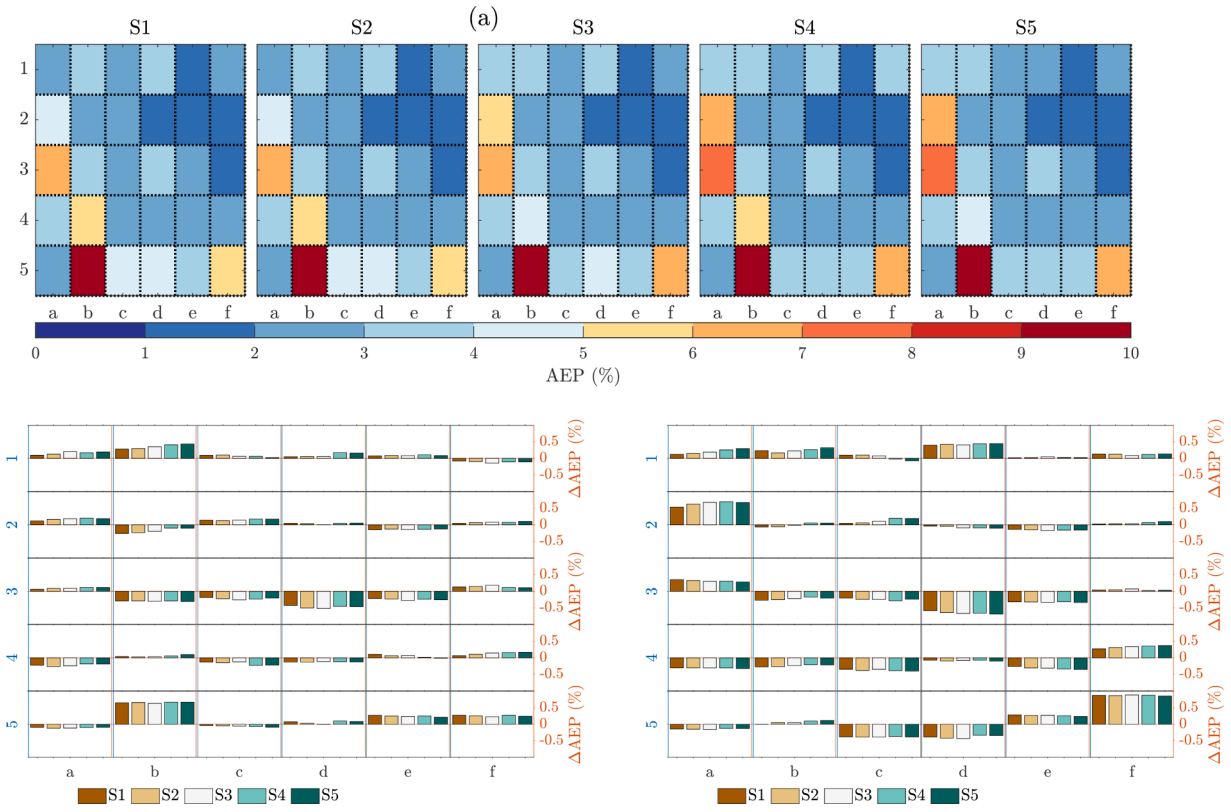

Fig. 10. (a) Distribution of the annual energy production (AEP) by weather pattern for S1–S5 in P-0; (b) projected change for P-I; and (c) as (b) but for P-II.

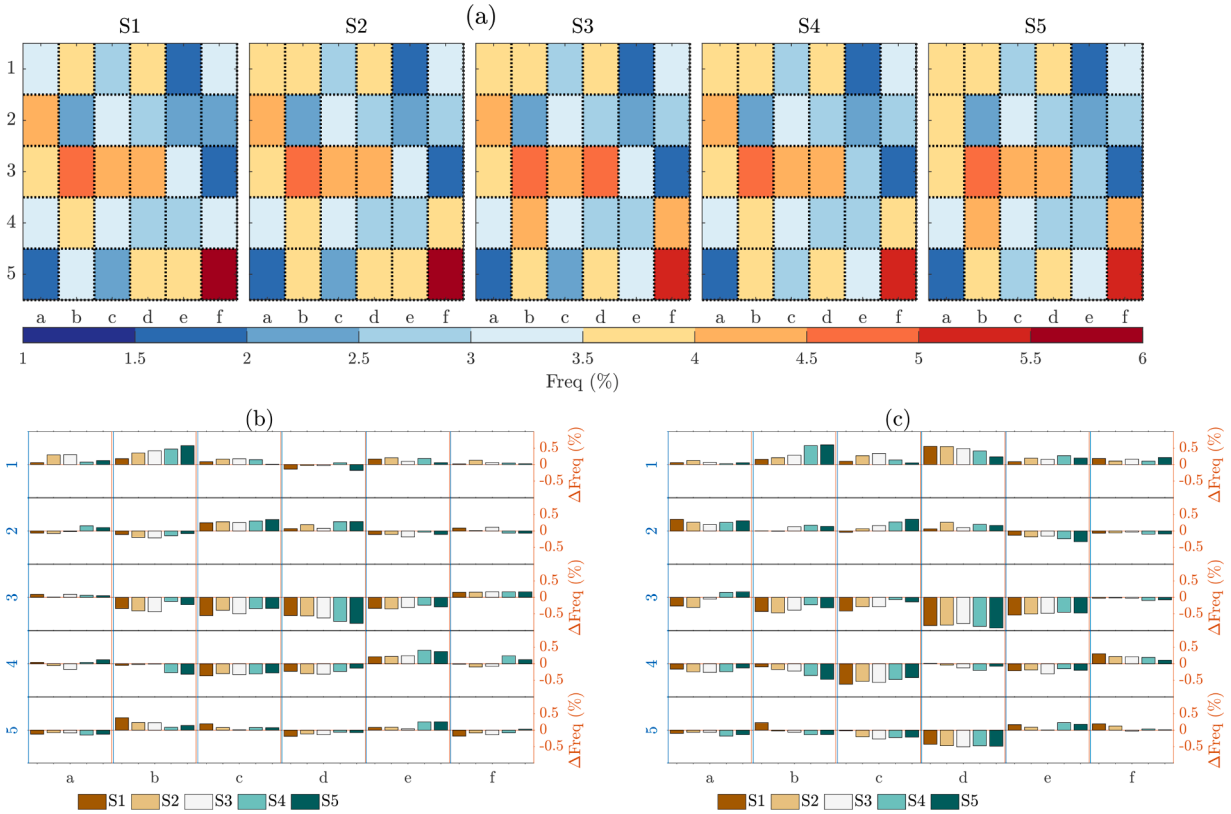

Fig. 11. (a) Distribution of ramp up events by weather pattern for S1–S5 in P-0; (b) projected change for P-I; and (c) as (b) but for P-II.

comprises a very strong low pressure system north of Europe with strong westerly winds. Pattern a3, with a strong south-west to north-east pressure gradient and north-westerly winds, also contributes a significant fraction to overall AEP. Fig. 10(b) and (c) show the projected changes in the distribution of AEP for P-I and P-II, respectively. The most significant change in P-I is an increase in the contribution to AEP by b5. The weather patterns in the middle row of the SOM show primarily reducing contributions to AEP. The changes seen during P-II show interesting trends. In this case, the AEP contribution from b5 is hardly different from P-0. Much of the AEP has been redistributed in the form of an increase associated with patterns a2 (similar circulation pattern to a3, but with the high over the Atlantic and the low over Scandinavia displaced more to the north-east) and f5 (similar circulation pattern to b5 but with the high over southern Europe and the low north of the UK displaced further north) balanced by a decrease across the third and fourth rows of the SOM, in particular d5 (similar circulation pattern to b5 but with the high over southern Europe displaced more to the east and the low north of the UK displaced more to the west, so winds move from being mainly westerly to more south-westerly). Trends across the sites S1–S5 are very similar. These trends broadly reflect the changes in occurrence of the different weather patterns observed in Fig. 3.

6.2. Impact on wind power ramps

Fig. 11(a) shows the distribution of ramp up events during P-0 by weather pattern for sites S1 – S5. The greatest single number of ramp up events is seen for class f5. This is a relatively frequently occurring pattern as seen in Fig. 3, however, not as frequent as the similar pattern b5 which contributes far fewer ramp up events. Weather patterns in the centre of the SOM with weak pressure gradients are also associated with a relatively large number of ramp up events. Weather patterns dominated by high pressure systems, and thus low wind speeds, seen at the top right of the SOM, are associated with relatively few ramps and also contribute little to AEP as seen in Fig. 10(a). Fig. 11(b) shows the change in ramp up event distribution for P-I. The most notable change is a reduction in the occurrence of ramp up events associated with weak pressure gradients in the centre of the SOM. For period P-II, shown in Fig. 11(c), the trend is similar, with additional significant decreases in contributions from c4 and d5 where winds are driven by low pressure systems. An increase in ramp-up events is seen for the first row of the SOM with high pressure dominated systems and periods of low production. Trends across the sites S1 – S5 are broadly similar.

Fig. 12(a) shows the distribution of ramp down events during P-0 by weather pattern for sites S1 – S5. Trends are similar as the ramp up events seen in Fig. 11(a), though there is a larger proportion of ramps associated with weather patterns at the top and left of the SOM, especially a2, a3 and b4. These patterns are associated with relatively strong north-westerly winds and weakening low pressure systems which are known to contribute to ramp down events [24,44,45]. Fig. 12(b) and (c) show the changes projected for P-I and P-II, respectively. The changes seen are very similar to those expected for ramp up events in Fig. 11(b) and (c).

7. Discussions

Before concluding this paper, we would like to point out a few limitations of the present study.

7.1. Vertical extrapolation of near-surface wind speeds

In this study, we make use of wind speed data from the Euro-CORDEX project and only consider the RCP45 scenario. Even though for other projection scenarios (e.g., RCP26 and RCP85), the Euro-CORDEX database provides 100 m wind speed values, similar high-altitude data are not available for the RCP45 case. Thus, we had to extrapolate the 10 m wind speed values to 100 m, which is the hub height of a hypothetical wind turbine. We used the adiabatic logarithmic law of the wall, that is only valid for neutrally stratified conditions. For

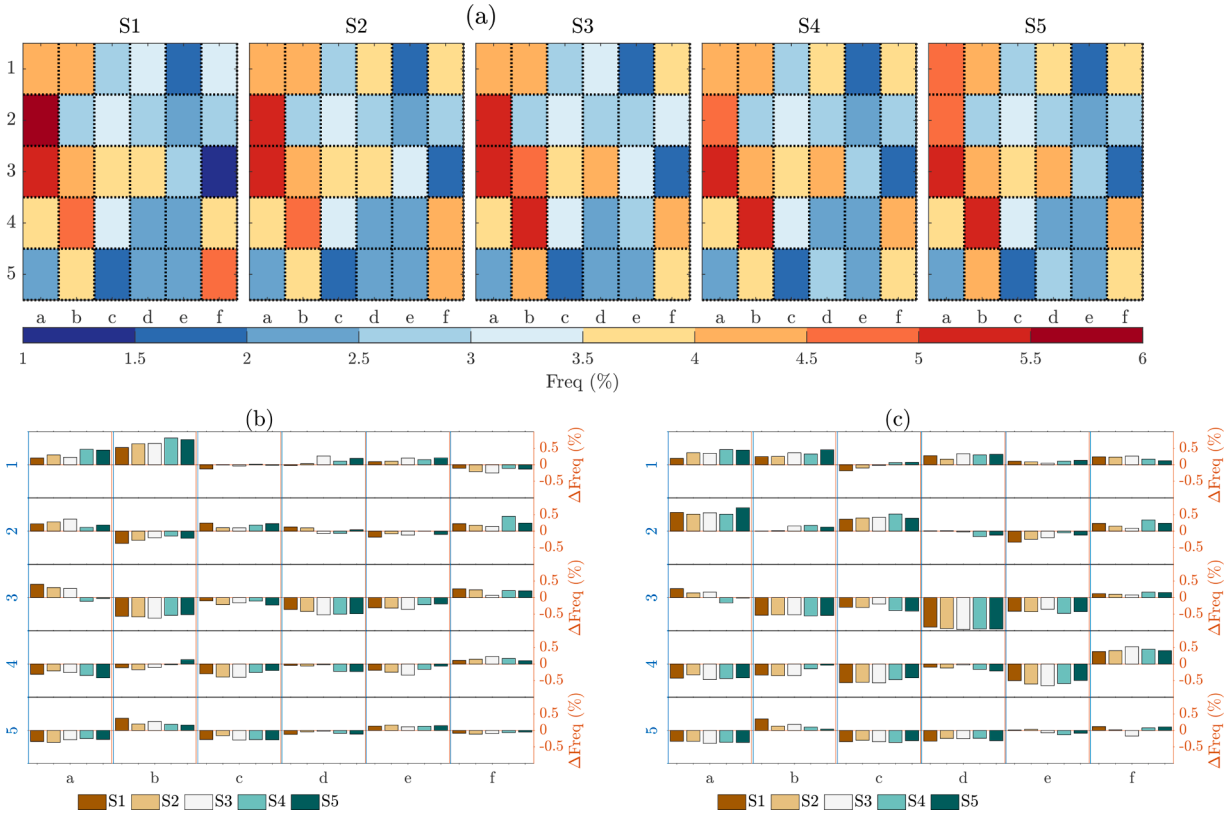

Fig. 12. (a) Distribution of ramp down events by weather pattern for S1–S5 in P-0, (b) projected change for P-I, and (c) as (b) but for P-II.

non-neutral conditions, one should use either the Monin-Obukhov (M-O) similarity formulation or one of its generalizations (e.g., [46]). Another viable approach would be to use the so-called geostrophic drag laws (e.g., [47]). For stable conditions, the boundary layer height could be very shallow. Furthermore, low-level jets are often present under stably stratified conditions. For such cases, the existing similarity formulations perform rather poorly (see [48] and the references therein). Given that the M-O and geostrophic drag law formulations require additional input variables (e.g., momentum flux, sensible heat flux, geostrophic wind speed), for simplicity, we opted to use the adiabatic logarithmic law in this study.

7.2. Notable differences in CMIP5 and CMIP6 datasets

All the statistical analyses of the present study are based on the Euro-CORDEX dataset downscaled from the CMIP5 runs. Recently, coarse-resolution data from the next-generation CMIP6 project have become publicly available. A few studies [49–51] have already compared the trends of projected wind power production based on CMIP5 and CMIP6 datasets. Several significant differences have been reported. For example, in contrast to CMIP5, CMIP6 predicts a decline in wind resources for Northern Europe and most of Europe by the end of the century (SSP5-8.5 scenario). At the same time, CMIP6 shows an increase in wind resources during future summers in some regions of southern Europe, whereas CMIP5 projects the opposite trend.

To the best of our knowledge, recent studies have yet to investigate the trends of wind ramps in CMIP6. Once downscaled (high-resolution) CMIP6 datasets become available, we will investigate this problem and revisit other science questions addressed in our current paper.

7.3. Thermodynamic effects

The change in projected wind energy is influenced not only due to the change in dynamics of large-scale meteorological systems but also determined by atmospheric thermodynamics. Ohba [19] investigated the influence of thermodynamics when studying wind ramp phenomena over Japan. In our future work, we intend to extend the current study to include thermodynamical influences.

8. Conclusions and recommendations

In this work, future changes in weather pattern occurrence, wind power production and wind power ramps have been analysed based on CORDEX data derived from the output from an ensemble of model used as part of CMIP5 to predict the future regional climate under the RCP4.5 scenario. A SOM was used to classify MLSP data into 30 discrete weather patterns to better understand the association between circulation patterns and wind power production and wind power ramps. The CORDEX data analysed were divided into three periods: a historic period (P-0), a near future period (P-I) and a far future period (P-II).

An increase was projected in the occurrence of weather patterns associated with high-pressure systems and north-easterly flows. By contrast, there was projected to be a reduction in the frequency of weather patterns associated with low-pressure systems and weak spatial pressure gradients.

Five North Sea sites, characteristic of offshore wind farms, were chosen to further study the spatial characteristics of wind power production and wind power ramps. Overall, based on the CMIP5 model ensemble, no significant change in wind power capacity factor was seen over the entire study period (P0, P-I and P-II), although there was tentative evidence of a reduction in wind power ramps.

Annual energy production is projected to be dominated by a small number of weather patterns with westerly, south-westerly or north-westerly winds. Changes in patterns of production in a future climate are not entirely monotonic, but production is projected to become less from westerly winds and more from south-westerly and north-westerly flows.

Ramp up events are primarily associated with strong south-westerly winds or weather patterns with a weak pressure gradient. Ramp down events have a stronger association with more north-westerly flow. The most notable change in a future climate is a reduction in ramp up events associated with weak pressure gradients.

The findings of this work are based on the assumption that a fixed number of weather patterns can be used to classify circulation patterns which are valid over a long period where the climate is changing. Further work is required to determine the validity of this assumption.

Declaration of Competing Interest

The authors declare that they have no known competing financial interests or personal relationships that could have appeared to influence the work reported in this paper.

Data availability

Data will be made available on request.

References

[1] IRENA Climate Change and Renewable Energy, National Policies and the Role of Communities, Cities and Regions. (Report to the G20 Climate Sustainability working group (CSWG)), International Renewable Energy Agency, Abu Dhabi, 2019.
[2] WindEurope, Wind in Power 2019, Annual Combined Onshore and Offshore Wind Energy Statistics, 2019.
[3] WindEurope, Offshore Wind Energy 2022 Mid-Year Statistics, 2022.
[4] S. Outten, I. Esau, Extreme winds over europe in the ensembles regional climate models, Atmos. Chem. Phys 13 (10) (2013) 5163–5172.
[5] A. Belušić Vozila, I. Güttler, B. Ahrens, A. Obermann-Hellhund, M. Telišman Prtenjak, Wind over the adriatic region in CORDEX climate change scenarios, J. Geophys. Res. Atmos. 124 (1) (2019) 110–130.
[6] J. Moemken, M. Reyers, H. Feldmann, J.G. Pinto, Future changes of wind speed and wind energy potentials in EURO-CORDEX ensemble simulations, J. Geophys. Res. Atmos. 123 (12) (2018) 6373–6389.
[7] J. Moemken, M. Reyers, H. Feldmann, J.G. Pinto, Wind speed and wind energy potentials in EURO-CORDEX ensemble simulations: evaluation, bias-correction and future changes. EGU General Assembly Conference Abstracts Vol. 19, 2017, p. 13305.
[8] B. Rockel, K. Woth, Extremes of near-surface wind speed over europe and their future changes as estimated from an ensemble of RCM simulations, Clim. Change 81 (1) (2007) 267–280.
[9] A. Höglund, M. Meier, B. Broman, E. Kriezi, Validation and correction of regionalised ERA-40 wind fields over the Baltic Sea using the Rossby Centre Atmosphere model RCA3.0, SMHI, 2009.
[10] S.C. Pryor, R. Barthelmie, Climate change impacts on wind energy: a review, Renew. Sustain. Energy Rev. 14 (1) (2010) 430–437.
[11] I. Tobin, R. Vautard, I. Balog, F.-M. Bréon, S. Jerez, P.M. Ruti, F. Thais, M. Vrac, P. Yiou, Assessing climate change impacts on european wind energy from ensembles high-resolution climate projections, Clim. Change 128 (1-2) (2015) 99–112.
[12] I. Koletsis, V. Kotroni, K. Lagouvardos, T. Soukissian, Assessment of offshore wind speed and power potential over the mediterranean and the black seas under future climate changes, Renew. Sustain. Energy Rev. 60 (2016) 234–245.
[13] M. Reyers, J. Moemken, J.G. Pinto, Future changes of wind energy potentials over Europe in a large CMIP5 multi-model ensemble, Int. J. Climatol. 36 (2) (2016) 783–796.
[14] J. Weber, F. Gotzens, D. Witthaut, Impact of strong climate change on the statistics of wind power generation in Europe, Energy Procedia 153 (2018) 22–28.
[15] R. Davy, N. Gnatiuk, L. Pettersson, L. Bobylev, Climate change impacts on wind energy potential in the european domain with a focus on the black sea, Renew. Sustain. Energy Rev. 81 (2018) 1652–1659.
[16] D.P. Van Vuuren, J. Edmonds, M. Kainuma, K. Riahi, A. Thomson, K. Hibbard, G. C. Hurtt, T. Kram, V. Krey, J.-F. Lamarque, et al., The representative concentration pathways: an overview, Climatic Change 109 (1) (2011) 5–31.
[17] G.P. Harrison, L.C. Cradden, J.P. Chick, Preliminary assessment of climate change impacts on the uk onshore wind energy resource, Energy Sources, Part A 30 (14-15) (2008) 1286–1299.
[18] S. Watson, Quantifying the variability of wind energy, Wiley Interdiscip. Rev. Energy Environ. 3 (4) (2014) 330–342.
[19] M. Ohba, The impact of global warming on wind energy resources and ramp events in Japan, Atmosphere 10 (5) (2019) 265.
[20] D.J. Brayshaw, A. Troccoli, R. Fordham, J. Methven, The impact of large scale atmospheric circulation patterns on wind power generation and its potential predictability: a case study over the UK, Renew. Energy 36 (8) (2011) 2087–2096.

[21] J.M. Garrido-Perez, C. Ordóñez, D. Barriopedro, R. García-Herrera, D. Paredes, Impact of weather regimes on wind power variability in western europe, Appl. Energy 264 (2020) 114731.
[22] T. Kohonen, Self-Organizing Maps Vol. 30, Springer Science & Business Media, 2012.
[23] B.R. Cheneka, S.J. Watson, S. Basu, The impact of weather patterns on offshore wind power production, J. Phys. Conf. Ser. 1618 (2020) 062032.
[24] B.R. Cheneka, S.J. Watson, S. Basu, Associating synoptic-scale weather patterns with aggregated offshore wind power production and ramps, Energies 14 (13) (2021) 3903.
[25] ESGF, Esgf@liu in cooperation with SMHI, 2021, https://esg-dn1.nsc.liu.se/search/cmip5.
[26] D. Jacob, J. Petersen, B. Eggert, A. Alias, O.B. Christensen, L.M. Bouwer, A. Braun, A. Colette, M. Déqué, G. Georgievski, et al., EURO-CORDEX: new high-resolution climate change projections for european impact research, Reg. Environ. Change 14 (2) (2014) 563–578.
[27] R. Knutti, J. Sedláček, Robustness and uncertainties in the new CMIP5 climate model projections, Nat. Clim. Change 3 (4) (2013) 369–373.
[28] A. Voldoire, E. Sanchez-Gomez, D.S. y Mélia, B. Decharme, C. Cassou, S. Sénési, S. Valcke, I. Beau, A. Alias, M. Chevallier, et al., The CNRM-CM5.1 global climate model: description and basic evaluation, Clim. Dyn. 40 (9-10) (2013) 2091–2121.
[29] W. Hazeleger, X. Wang, C. Severijns, S. Ştefănescu, R. Bintanja, A. Sterl, K. Wyser, T. Semmler, S. Yang, B. Van den Hurk, et al., EC-earth V2.2: description and validation of a new seamless earth system prediction model, Clim. Dyn. 39 (11) (2012) 2611–2629.
[30] O. Marti, P. Braconnot, J.-L. Dufresne, J. Bellier, R. Benshila, S. Bony, P. Brockmann, P. Cadule, A. Caubel, F. Codron, et al., Key features of the IPSL ocean atmosphere model and its sensitivity to atmospheric resolution, Clim. Dyn. 34 (1) (2010) 1–26.
[31] C. Jones, J. Hughes, N. Bellouin, S. Hardiman, G. Jones, J. Knight, S. Liddicoat, F. O'connor, R.J. Andres, C. Bell, et al., The HadGEM2-ES implementation of CMIP5 centennial simulations, Geosci. Model Dev. 4 (2011) 543–570.
[32] M.A. Giorgetta, J. Jungclaus, C.H. Reick, S. Legutke, J. Bader, M. Böttinger, V. Brovkin, T. Crueger, M. Esch, K. Fieg, et al., Climate and carbon cycle changes from 1850 to 2100 in MPI-ESM simulations for the coupled model intercomparison project phase 5, J. Adv. Model. Earth Syst. 5 (3) (2013) 572–597.
[33] M. Bentsen, I. Bethke, J. Debernard, T. Iversen, A. Kirkevåg, Ø. Seland, H. Drange, C. Roelandt, I. Seierstad, C. Hoose, et al., The norwegian earth system model, NorESM1-M-Part 1: description and basic evaluation, GMDD 5 (3) (2012) 2843–2931.
[34] T. Iversen, M. Bentsen, I. Bethke, J. Debernard, A. Kirkevåg, Ø. Seland, H. Drange, J. Kristjansson, I. Medhaug, M. Sand, et al., The norwegian earth system model, NorESM1-M–Part 2: climate response and scenario projections, Geosci. Model Dev. 6, 389–415, 2013.
[35] S. Emeis, Wind Energy Meteorology: Atmospheric Physics for Wind Power Generation, Springer, 2018.
[36] C. Desmond, J. Murphy, L. Blonk, W. Haans, Description of an 8 MW reference wind turbine. Journal of Physics: Conference Series Vol. 753, IOP Publishing, 2016, p. 092013.
[37] B.R. Cheneka, S.J. Watson, S. Basu, A simple methodology to detect and quantify wind power ramps, Wind Energy Sci. 5 (4) (2020) 1731–1741.
[38] L. Bianco, I.V. Djalalova, J.M. Wilczak, J. Cline, S. Calvert, E. Konopleva-Akish, C. Finley, J. Freedman, A wind energy ramp tool and metric for measuring the skill of numerical weather prediction models, Weather Forecast. 31 (4) (2016) 1137–1156.
[39] C. Gallego-Castillo, A. Cuerva-Tejero, O. Lopez-Garcia, A review on the recent history of wind power ramp forecasting, Renew. Sustain. Energy Rev. 52 (2015) 1148–1157.
[40] R. Sevlian, R. Rajagopal, Detection and statistics of wind power ramps, IEEE Trans. Power Syst. 28 (4) (2013) 3610–3620.
[41] A. Bossavy, R. Girard, G. Kariniotakis, Forecasting uncertainty related to ramps of wind power production. European Wind Energy Conference and Exhibition 2010, EWEC 2010 Vol. 2, European Wind Energy Association, 2010, pp. 9–pages.
[42] T. Kohonen, J. Hynninen, J. Kangas, J. Laaksonen, SOM PAK: The Self-Organizing Map Program Package. Technical Report, Citeseer, 1996.
[43] J.W. Sammon, A nonlinear mapping for data structure analysis, IEEE Trans. Comput. 100 (5) (1969) 401–409.
[44] C. Ferreira, J. Gama, L. Matias, A. Botterud, J. Wang, A Survey on Wind Power Ramp Forecasting. Technical Report, Argonne National Lab.(ANL), Argonne, IL (United States), 2011.
[45] M. Ohba, S. Kadokura, D. Nohara, Impacts of synoptic circulation patterns on wind power ramp events in East Japan, Renew. Energy 96 (2016) 591–602.
[46] S.-E. Gryning, E. Batchvarova, B. Brümmer, H. Jørgensen, S. Larsen, On the extension of the wind profile over homogeneous terrain beyond the surface boundary layer, Boundary-Layer Meteorol. 124 (2007) 251–268.
[47] S.S. Zilitinkevich, I.N. Esau, Resistance and heat-transfer laws for stable and neutral planetary boundary layers: old theory advanced and re-evaluated, Q. J. R. Meteorol. Soc. 131 (2005) 1863–1892.
[48] S. Basu, Vertical wind speed profiles in atmospheric boundary layer flows, in: T. Letcher (Ed.), Wind Energy Engineering: A Handbook for Onshore and Offshore Wind Turbines, second ed., Elsevier, 2022.
[49] D. Carvalho, A. Rocha, X. Costoya, M. DeCastro, M. Gómez-Gesteira, Wind energy resource over europe under CMIP6 future climate projections: what changes from CMIP5 to CMIP6, Renew. Sustain. Energy Rev. 151 (2021) 111594.
[50] J. Wohland, Process-based climate change assessment for european winds using EURO-CORDEX and global models, Environ. Res. Lett. 17 (12) (2022) 124047.
[51] A.N. Hahmann, O. García-Santiago, A. Peña, Current and future wind energy resources in the North Sea according to CMIP6, Wind Energy Sci. 7 (6) (2022) 2373–2391.